Available online at www.sciencedirect.com
SCIENCE DIRECT®
Comput. Methods Appl. Mech. Engrg. 195 (2006) 4433–4447
Computer methods in applied mechanics and engineering
www.elsevier.com/locate/cma

Time step restrictions using semi-explicit methods for the incompressible Navier–Stokes equations

Wendy Kress, Per Lötstedt *

Division of Scientific Computing, Department of Information Technology, Uppsala University, Box 337, SE-75105 Uppsala, Sweden

Received 2 August 2004; received in revised form 7 August 2005; accepted 16 September 2005

Abstract

The incompressible Navier–Stokes equations are discretized in space by a finite difference method and integrated in time by the method of lines and a semi-explicit method. In each time step a set of systems of linear equations has to be solved. The size of the time steps is restricted by stability and accuracy of the time-stepping scheme, and convergence of the iterative methods for the solution of the systems of equations. The stability is investigated with a linear model equation derived from the Navier–Stokes equations on Cartesian grids. The resolution in space and time is estimated from turbulent flow physics. The convergence of the iterative solvers is discussed with respect to the time steps. The stability constraints obtained from the model equation are compared to results for a semi-explicit integrator of the Navier–Stokes equations with good agreement. The most restrictive bound on the time step is given by accuracy, stability, or convergence depending on the flow conditions and the numerical method.

MSC: 65M06; 65M12

Keywords: Incompressible flow; Iterative solution; Semi-explicit method; Accuracy constraints; Stability

1. Introduction

Direct simulation of the Navier–Stokes equations (DNS) is a computational tool to study turbulent flow. Spectral and pseudospectral methods have been developed for this purpose but they are restricted to simple geometries such as straight channels. For more complex problems a finite difference or finite element method is more suitable. Examples of such methods are found, e.g., in [5,7,32]. DNS calculations are computationally very demanding with long execution times and large memory requirements. One important issue is how the equations are discretized in space. Another question is how to integrate the equations in time. Given the space discretization, the time derivatives are usually approximated by a standard method for ordinary differential equations [21] or a combination of such methods. The scheme may be implicit [12,42], semi-implicit [17,42], semi-explicit [7,24], or explicit [13,41]. Then in each time step there are in general one or more systems of linear equations to solve for the velocity and the pressure. Preferably the systems of equations are solved by iterative methods since they are superior in efficiency and memory requirements for large problems. In this solution strategy, the time step shall be chosen so that

1. The integration is stable.
2. The solution is sufficiently accurate in time.
3. The iterative solvers converge quickly.

* Corresponding author. Tel.: +46 18 471 2972; fax: +46 18 523049.
E-mail address: perl@it.uu.se (P. Lötstedt).

0045-7825/$ - see front matter
doi:10.1016/j.cma.2005.09.009

Less computational work is spent in a time interval if the time steps are long, but long time steps may be in conflict with all three requirements above. Ideally the solution algorithm should be such that only accuracy restricts the time step but this is seldom possible for nonlinear problems. In this paper we investigate this matter and derive bounds on the time step imposed by the stability, accuracy, and convergence for semi-explicit methods in general and the integration method with the finite difference space discretization in [7] in particular.

The Navier–Stokes equations for incompressible flow in two dimensions (2D) in the primitive variables are as follows. Let u and v be the velocity components in the x- and y-directions, respectively, p the pressure, and ν the kinematic viscosity. The Reynolds number is defined by $Re = u_b\ell/\nu$ for some characteristic velocity u_b and length scale ℓ. Let $\mathbf{w} = (u, v)^{\mathrm{T}}$. Introduce the nonlinear and linear terms

$$\mathcal{N}(\mathbf{w}) = (\mathbf{w}\cdot\nabla)\mathbf{w}, \quad \mathcal{L}(\mathbf{w}, p) = \nabla p - Re^{-1}\Delta\mathbf{w}.$$

Then the Navier–Stokes equations in 2D are

$$\partial_t\mathbf{w} + \mathcal{N}(\mathbf{w}) + \mathcal{L}(\mathbf{w}, p) = 0, \tag{1}$$

$$\nabla\cdot\mathbf{w} = 0. \tag{2}$$

The space discretizations of $\mathcal{N}$ and $\mathcal{L}$ in (1) and $\nabla\cdot$ in (2) are denoted by $\mathcal{N}_h$ and $\mathcal{L}_h$ and $\nabla_h\cdot$. Suppose that the solution in space $\mathbf{w}^n$ is known at time t^n and that we intend to compute $\mathbf{w}^{n+1}$ at t^{n+1} with the time step $\Delta t = t^{n+1} - t^n$. In an implicit method, $\mathbf{w}^{n+1}$ fulfills

$$\mathbf{w}^{n+1} + c_1\Delta t\mathcal{N}_h(\mathbf{w}^{n+1}) + c_2\Delta t\mathcal{L}_h(\mathbf{w}^{n+1}, p) = \mathbf{b}^n_{\mathrm{impl}}, \tag{3}$$

where c_1 and c_2 are constants depending on the method and $\mathbf{b}^n_{\mathrm{impl}}$ depends on previous solutions $\mathbf{w}^n$, $\mathbf{w}^{n-1}, \ldots$ In a semi-implicit method the convection term is linearized by introducing a previous solution $\bar{\mathbf{w}}$ in the iterations in the approximation of $\mathcal{N}_h$ such that $\mathcal{N}_h(\mathbf{w}^{n+1}) \approx (\bar{\mathbf{w}}\cdot\nabla)\mathbf{w}^{n+1}$. The nonlinear term is treated explicitly in a semi-explicit method

$$\mathbf{w}^{n+1} + c_1\Delta t\mathcal{L}_h(\mathbf{w}^{n+1}, p) = \mathbf{b}^n_{\mathrm{sexpl}}, \tag{4}$$

where $\mathbf{b}^n_{\mathrm{sexpl}}$ includes $\mathcal{N}_h$ and depends on $\mathbf{w}^n, \mathbf{w}^{n-1}, \ldots$ In an explicit scheme, also the linear term is evaluated from previous solutions

$$\mathbf{w}^{n+1} = \mathbf{b}^n_{\mathrm{expl}}, \tag{5}$$

so that $\mathbf{w}^{n+1}$ is updated without the need to solve a system of equations for the velocity.

The integration method in [7,8,33] is semi-explicit as in (4) and second order accurate with a fourth order accurate compact finite difference discretization of the space derivatives in 2D [9,27]. The solution is expanded in a Fourier series in the third dimension [8]. The system of linear equations for $\mathbf{w}^{n+1}$ and p in each time step is solved in one outer and two inner iterations. The analysis developed here is applied to this method as an example. Although the stability analysis is restricted to this particular space discretization on Cartesian equidistant grids including a linearization, we believe that the trends are more generally applicable to other spatial approximations. The stability constraints are e.g., modified only slightly for a second order method.

There are different options to satisfy the incompressibility condition (2) and to determine the pressure p at t^{n+1}. One possibility is to compute a provisional $\mathbf{w}^*$ and then add a correction so that (2) is satisfied in a pressure correction method or a projection method [4,6,13,15,41,23]. An approximate factorization is determined in a fractional step method to obtain two simpler systems of equations [11,14,26,36]. Another way is to solve (3) or (4) and (2) for $\mathbf{w}^{n+1}$ and p simultaneously and iterate until convergence as in [7,17,43].

The stability and accuracy of semi-explicit (or mixed explicit/implicit) integration methods for the incompressible Navier–Stokes equations are investigated in [24]. The length of the time steps is studied in [12] for turbulent flow with an implicit treatment of $\mathcal{N}_h$ and $\mathcal{L}_h$. A discussion of appropriate time steps for accuracy and stability in turbulent flow is found in [19]. The stability and accuracy of combinations of implicit and explicit methods for one-dimensional, scalar convection–diffusion equations are evaluated in [3].

The time and space discretizations are discussed in Section 2. The time derivative is approximated either by a backward differentiation formula (BDF) or an Adams method. The nonlinear convection term is extrapolated from old solutions or advanced by an explicit Adams method. The analysis of the stability of the discretization in 2D is based on the Oseen equations with frozen velocity coefficients in the nonlinear term $\mathcal{N}_h$ in Section 3. Stability of the particular semi-explicit scheme in [7] is studied in [20] using Fourier analysis. This analysis is generalized here to other classes of semi-explicit methods. If stability problems are indicated using Fourier analysis with locally frozen coefficients, then such trouble is likely to occur also in the nonlinear problem. The model for the stability analysis is validated by comparison of the predictions with the results from calculations with the Navier–Stokes solver [7] in a straight channel. The methodology is easily applicable to other space discretizations. The maximum lengths of the temporal and spatial steps for sufficient accuracy are estimated in

Section 4. The assumption is that the scales in time and space in turbulent flow must be resolved by a certain number of discrete points depending on the order of accuracy of the discretization. The scales are estimated from basic physical relations at the solid wall. The separate stages of the iterative solution and their dependence on the time step are discussed in Section 5. Conclusions are drawn in the final section.

2. Discretization

Eq. (1) is discretized in time either by an implicit method (3), a semi-explicit method (4) or an explicit method (5). These methods are here described for members of two classes of linear multistep methods: Adams methods and backward differentiation formulas (BDF) [21]. Linear multistep methods have the advantage compared to Runge–Kutta (RK) methods that fewer evaluations of the expensive space derivatives per time step are required.

An implicit scheme is obtained if a BDF-scheme or an implicit Adams–Moulton scheme is applied to (1). The velocity and pressure vectors satisfy a nonlinear system of Eq. (3) and a discretization of (2) in each time step.

One family of semi-explicit methods of order r is obtained by extrapolating $\mathcal{N}_h(\mathbf{w})$ from time t^{n-r+1} up to t^n with an $(r-1)$th order polynomial to t^{n+1} and applying the rth order backward differentiation formula (BDFr) to the linear terms to arrive at

$$\sum_{j=0}^{r} \alpha_j \mathbf{w}^{n+1-j} + \Delta t \beta_0^i \mathcal{L}_h(\mathbf{w}^{n+1}, p^{n+1}) = -\Delta t \sum_{j=1}^{r} \beta_j^e \mathcal{N}_h(\mathbf{w}^{n+1-j}). \tag{6}$$

The coefficients α_j are given by BDFr and the coefficients β_j^e are defined by the extrapolation

$$\mathbf{w}^{n+1} = \sum_{j=1}^{r} \beta_j^e \mathbf{w}^{n+1-j} + \mathcal{O}(\Delta t^r),$$

and $\beta_0^i = 1$. The coefficients in (6) up to order $r = 4$ are given in Table 1. In addition, $\mathbf{w}^{n+1}$ and p are such that $\mathbf{w}^{n+1}$ satisfies a discretization of the divergence equation in (2). The result is a system of linear equations for $\mathbf{w}^{n+1}$ and p^{n+1}. The integration is started at t^0 with $r = 1$.

Another class of time discretizations, based on Adams methods, is derived from integrating (1) in time

$$\mathbf{w}^{n+1} - \mathbf{w}^n = -\int_{t^n}^{t^{n+1}} \mathcal{L}_h(\mathbf{w}, p)\mathrm{d}t - \int_{t^n}^{t^{n+1}} \mathcal{N}_h(\mathbf{w})\mathrm{d}t. \tag{7}$$

The integral with the nonlinearity is approximated by an explicit Adams–Bashforth method and the integral with the linear integrand by an implicit Adams–Moulton method [21]. The resulting formula of order r is

$$\mathbf{w}^{n+1} - \mathbf{w}^n = -\Delta t \sum_{j=0}^{r-1} \beta_j^i \mathcal{L}_h(\mathbf{w}^{n+1-j}, p^{n+1-j}) - \Delta t \sum_{j=1}^{r} \beta_j^e \mathcal{N}_h(\mathbf{w}^{n+1-j}), \tag{8}$$

i.e., $\alpha_0 = 1$ and $\alpha_1 = -1$. The coefficients for $2 \leqslant r \leqslant 4$ are given in Table 2. A common combination is the Adams–Bashforth method of second order and the implicit trapezoidal (or Crank–Nicolson) method [26,30]. The last integral in (7) is easily evaluated by an explicit RK scheme at the expense of additional calculations of $\mathcal{N}_h$ at interior stages between t^n and t^{n+1}. The Crank–Nicolson scheme is combined with an explicit RK method in [5] and a more elaborate RK method in [29].

Table 1
Coefficients for BDF methods (6)

	α_0	α_1	α_2	α_3	α_4	β_1^e	β_2^e	β_3^e	β_4^e
BDF1	1	−1				1			
BDF2	3/2	−2	1/2			2	−1		
BDF3	11/6	−3	3/2	−1/3		3	−3	1	
BDF4	25/12	−4	3	−4/3	1/4	4	−6	4	−1

Table 2
Coefficients for Adams methods (8)

	β_0^i	β_1^i	β_2^i	β_3^i	β_1^e	β_2^e	β_3^e	β_4^e
Adams2	1/2	1/2			3/2	−1/2		
Adams3	5/12	8/12	−1/12		23/12	−16/12	5/12	
Adams4	9/24	19/24	−5/24	1/24	55/24	59/24	37/24	−9/24

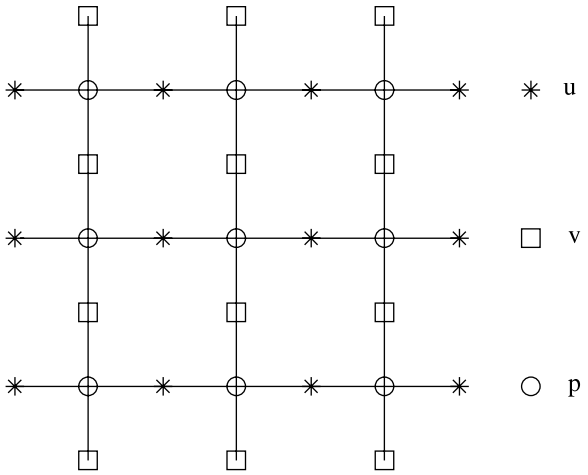

Fig. 1. A staggered grid.

In the stability analysis in the next section, the space discretization is assumed to be a fourth order accurate compact finite difference method as in [7] inspired by [28]. There, the gradient and divergence operators are discretized with the help of fourth order compact operators of the form

$$\frac{1}{24}f'_{i-1}+\frac{11}{12}f'_i+\frac{1}{24}f'_{i+1}=\frac{1}{\Delta x}(f_{i+1/2}-f_{i-1/2}), \tag{9}$$

$$\frac{1}{6}f'_{i-1}+\frac{2}{3}f'_i+\frac{1}{6}f'_{i+1}=\frac{1}{2\Delta x}(f_{i+1}-f_{i-1}) \tag{10}$$

and for the Laplacian, formulas of the type

$$\frac{1}{12}f''_{i-1}+\frac{10}{12}f''_i+\frac{1}{12}f''_{i+1}=\frac{1}{\Delta x^2}(f_{i-1}-2f_i+f_{i+1}) \tag{11}$$

are used on a Cartesian grid. Together with appropriate numerical boundary conditions, Eqs. (9)–(11) can be written in matrix form as $Pf'=Qf$, $\widetilde{P}f'=\widetilde{Q}f$ and $Rf''=Sf$, respectively. The components u, v and p are calculated at different points on a staggered grid, as depicted in Fig. 1. On a Cartesian grid, the fourth order discretization becomes

$$\begin{aligned}
\mathscr{L}_h(\mathbf{w},p)&=\begin{pmatrix}P_x^{-1}Q_xp-Re^{-1}(R_x^{-1}S_x+R_y^{-1}S_y)u\\ P_y^{-1}Q_yp-Re^{-1}(R_x^{-1}S_x+R_y^{-1}S_y)v\end{pmatrix},\\
\mathscr{N}_h(\mathbf{w})&=\begin{pmatrix}u\widetilde{P}_x^{-1}\widetilde{Q}_xu+Ev\widetilde{P}_y^{-1}\widetilde{Q}_yu\\ Eu\widetilde{P}_x^{-1}\widetilde{Q}_xv+v\widetilde{P}_y^{-1}\widetilde{Q}_yv\end{pmatrix},\\
\nabla_h\cdot\mathbf{w}&=P_x^{-1}Q_xu+P_y^{-1}Q_yv,
\end{aligned} \tag{12}$$

where E is an interpolation operator between the u and v points, see [9]. A standard second order discretization is achieved by replacing P, $\widetilde{P}$ and R with identity operators.

3. Stability analysis

The Navier–Stokes equations are linearized by freezing the velocity $\mathbf{w}$ in front of the gradient in the nonlinear term to obtain the Oseen equations as in [20]

$$\mathbf{w}_t+(\bar{\mathbf{w}}\cdot\nabla)\mathbf{w}+\mathscr{L}(\mathbf{w},p)=0, \tag{13}$$

$$\nabla\cdot\mathbf{w}=0, \tag{14}$$

where $\bar{\mathbf{w}}=(\bar{u},\bar{v})$ consists of two constants. A rectangular physical domain with periodic boundary conditions is discretized with a Cartesian grid with constant step sizes Δx and Δy. The space discretization (12) and a Fourier transformation in x and y is used to arrive at a system of equations for the transformed variables $\hat{\mathbf{w}}=(\hat{u},\hat{v})^{\mathrm{T}}$ and $\hat{p}$. Let ω_1 and ω_2 be the discrete wavenumbers in the x- and y-directions and introduce the notation

$$\begin{aligned}
&\xi_1=\omega_1\Delta x,\quad \xi_2=\omega_2\Delta y,\quad 0\leqslant|\xi_1|,\quad |\xi_2|\leqslant\pi,\\
&\lambda_x=\Delta t/\Delta x,\quad \lambda_y=\Delta t/\Delta y,\quad s_j=\sin\xi_j/2,\quad c_j=\cos\xi_j/2,\quad j=1,2.
\end{aligned}$$

The CFL-numbers in the x- and y-directions are $\bar{u}\lambda_x$ and $\bar{v}\lambda_y$. For the Fourier transformation of the equations of fourth order accuracy the following coefficients are introduced:

$$a_1 = \frac{3\mathrm{i}\sin\xi_1}{2+\cos\xi_1} = \frac{6\mathrm{i}s_1c_1}{1+2c_1^2}, \quad a_2 = \frac{3\mathrm{i}\sin\xi_2}{2+\cos\xi_2} = \frac{6\mathrm{i}s_2c_2}{1+2c_2^2}, \tag{15a}$$

$$b_1 = \frac{24\mathrm{i}s_1}{11+\cos\xi_1} = \frac{12\mathrm{i}s_1}{5+c_1^2}, \quad b_2 = \frac{24\mathrm{i}s_2}{11+\cos\xi_2} = \frac{12\mathrm{i}s_2}{5+c_2^2}, \tag{15b}$$

$$c_0 = 24\left(\frac{s_1^2}{5+\cos\xi_1} + \frac{\Delta x^2 s_2^2}{\Delta y^2(5+\cos\xi_2)}\right) = 12\left(\frac{s_1^2}{2+c_1^2} + \frac{\Delta x^2 s_2^2}{\Delta y^2(2+c_2^2)}\right), \tag{15c}$$

$$\theta = \frac{\Delta t}{Re\Delta x^2}. \tag{15d}$$

The standard, centered second order accurate space discretization generates the following coefficients:

$$a_1 = 2\mathrm{i}s_1c_1, \quad a_2 = 2\mathrm{i}s_2c_2, \tag{16a}$$

$$b_1 = 2\mathrm{i}s_1, \quad b_2 = 2\mathrm{i}s_2, \tag{16b}$$

$$c_0 = 4\left(s_1^2 + \Delta x^2 s_2^2/\Delta y^2\right). \tag{16c}$$

Then the Fourier transformed system for the variables $\hat{u}$, $\hat{v}$ and $\hat{p}$ is

$$\sum_{j=0}^{r}\alpha_j\hat{u}^{n+1-j} + (\bar{u}\lambda_x a_1 + \bar{v}\lambda_y a_2)\sum_{j=1}^{r}\beta_j^e\hat{u}^{n+1-j} + \lambda_x b_1\sum_{j=0}^{r-1}\beta_j^i\hat{p}^{n+1-j} + \theta c_0\sum_{j=0}^{r-1}\beta_j^i\hat{u}^{n+1-j} = 0, \tag{17a}$$

$$\sum_{j=0}^{r}\alpha_j\hat{v}^{n+1-j} + (\bar{u}\lambda_x a_1 + \bar{v}\lambda_y a_2)\sum_{j=1}^{r}\beta_j^e\hat{v}^{n+1-j} + \lambda_y b_2\sum_{j=0}^{r-1}\beta_j^i\hat{p}^{n+1-j} + \theta c_0\sum_{j=0}^{r-1}\beta_j^i\hat{v}^{n+1-j} = 0, \tag{17b}$$

$$b_1\hat{u}^{n+1} + b_2\hat{v}^{n+1} = 0. \tag{17c}$$

Multiply (17a) by b_1 and (17b) by b_2 and add them together. Since (17c) is satisfied by $\hat{u}^n$ and $\hat{v}^n$ for all $n \geqslant 1$, the equation for $\hat{p}^{n+1}$ is

$$(\lambda_x b_1^2 + \lambda_y b_2^2)\sum_{j=0}^{r-1}\beta_j^i\hat{p}^{n+1-j} = 0. \tag{18}$$

If at least one ξ_j, $j = 1, 2$, satisfies $\xi_j \neq 0$, then $\lambda_x b_1^2 + \lambda_y b_2^2 \neq 0$ and the sum in (18) vanishes. Then (17b) for $\hat{v}^{n+1}$ is identical to (17a) for $\hat{u}^{n+1}$. We can rewrite the first equation with $\beta_r^i = 0$ to obtain

$$(\alpha_0 + \beta_0^i\theta c_0)\hat{u}^{n+1} + \sum_{j=1}^{r}(\alpha_j + \beta_j^e(\bar{u}\lambda_x a_1 + \bar{v}\lambda_y a_2) + \beta_j^i\theta c_0)\hat{u}^{n+1-j} = 0.$$

For $\xi_1 = \xi_2 = 0$ the time-integration degenerates to

$$\sum_{j=0}^{r}\alpha_j\hat{u}^{n+1-j} = 0. \tag{19}$$

BDF methods are zero-stable for $1 \leqslant r \leqslant 6$ and all Adams methods have this property [21] and therefore the sequence $\hat{u}^n$ in (19) is stable for such r.

We can show that there is no parasitic odd–even oscillatory solution for the second and fourth order approximations, cf. [20]. Consider the steady state case in (17). The equations are the same for $\hat{u}$ and $\hat{v}$. We can assume the scaling $\sum_{j=1}^{r}\beta_j^e = \sum_{j=0}^{r-1}\beta_j^i = 1$. Since $\sum_{j=0}^{r}\alpha_j = 0$, the time-independent $\hat{u}$ fulfills

$$(\theta c_0 + \bar{u}\lambda_x a_1 + \bar{v}\lambda_y a_2)\hat{u} = 0.$$

With $\xi_1 = \xi_2 = \pi$ in (15) and (16) corresponding to the odd–even parasitic solution, the equation is

$$\theta c_0\hat{u} = 0$$

showing that no non-trivial solution exists.

The stability of the scheme when ξ_1 and ξ_2 are not both zero is determined by the roots of the polynomial

$$(\alpha_0 + \beta_0^i\theta c_0)z^r + \sum_{j=1}^{r}(\alpha_j + \beta_j^e(\bar{u}\lambda_x a_1 + \bar{v}\lambda_y a_2) + \beta_j^i\theta c_0)z^{r-j} = 0. \tag{20}$$

The scheme is stable if all roots z of the characteristic Eq. (20) satisfy $|z| \leqslant 1$ and if $|z| = 1$ then it is a simple root.

3.1. Stability domain for BDF2

Let $\vartheta = \theta c_0$. The characteristic equation for the second order BDF method, $r = 2$ in Table 1, is then given by

$$(1.5 + \vartheta)z^2 + 2(\xi - 1)z + (0.5 - \xi) = 0, \tag{21}$$

where we have introduced $\xi = \bar{u}\lambda_x a_1 + \bar{v}\lambda_y a_2$. The boundary of the stability domain is determined by calculating the values of ξ for $|z| = 1$. The method is stable for values of ξ inside the boundary. In addition, ξ is purely imaginary. Thus, we only consider an interval on the imaginary axis.

Proposition 1. *The characteristic Eq. (21) has stable solutions* $|z| \leqslant 1$ *for* ξ *in the interval* $[-\xi_*, \xi_*]$, *where*

$$\xi_* = \mathrm{i}\frac{\sqrt{3\vartheta(1+\vartheta)}(2+\vartheta) - \vartheta(1+\vartheta)}{\sqrt{2(3+\vartheta)\sqrt{3\vartheta(1+\vartheta)} + 3\vartheta}}.$$

Proof. With ξ_* purely imaginary, Eq. (21) together with $|z| = 1$ leads to three equations for the real and imaginary parts of z, $\Re(z)$ and $\Im(z)$, and $\Im(\xi_*)$

$$\begin{aligned}
&(1.5 + \vartheta)(\Re(z)^2 - \Im(z)^2) - 2(\Im(\xi_*)\Im(z) + \Re(z)) + 0.5 = 0,\\
&(1.5 + \vartheta)2\Re(z)\Im(z) + 2(\Im(\xi_*)\Re(z) - \Im(z)) - \Im(\xi_*) = 0,\\
&\Re(z)^2 + \Im(z)^2 = 1.
\end{aligned} \tag{22}$$

Taking into account symmetry, we consider only $\Im(\xi_*) \geqslant 0$. The solution to (22) is given by

$$\begin{aligned}
\Re(z) &= \frac{3 + \vartheta - \sqrt{3\vartheta(1+\vartheta)}}{3 + 2\vartheta},\\
\Im(z) &= \frac{\sqrt{2(3+\vartheta)\sqrt{3\vartheta(1+\vartheta)} + 3\vartheta}}{3 + 2\vartheta},\\
\Im(\xi_*) &= \frac{\sqrt{3\vartheta(1+\vartheta)}(2+\vartheta) - \vartheta(1+\vartheta)}{\sqrt{2(3+\vartheta)\sqrt{3\vartheta(1+\vartheta)} + 3\vartheta}}.
\end{aligned} \tag{23}$$

Only $z = 0.5$ is a double root. □

For fixed θ, the boundary of the stability domain in the $\bar{u}\lambda_x - \bar{v}\lambda_y$ plane is calculated by

$$\bar{u}\lambda_x = \min_{\omega_1,\omega_2}\left(-\bar{v}\lambda_y a_2/a_1 + \xi_*/a_1\right).$$

In Fig. 2, the boundary of the stability domain for different values of θ has been calculated. The scheme is stable for values of $(\bar{u}\lambda_x, \bar{v}\lambda_y)$ inside the lines depicted in the figure. The asymptotic behavior of ξ_* for large ϑ is $\Im(\xi_*) \sim \vartheta$ and for small ϑ, it is $\Im(\xi_*) \sim \vartheta^{\frac{1}{4}}$. Thus, we expect linear growth of the radius of the stability region for increasing θ and a decrease of the stability region like $\theta^{\frac{1}{4}}$ for decreasing θ.

The stability domains in Fig. 2 have been computed with the fourth order discretization (12), but are easily obtained for other finite difference approximations in space. If the second order scheme with Fourier coefficients (16), is chosen then the boundaries of the stability domains are slightly perturbed in the figure.

3.2. Stability domain for other methods

In addition to the BDF2 scheme implemented in [7,8], we examine the stability properties of a series of other semi-explicit multistep schemes: BDF1, BDF3, BDF4, Adams2, Adams3 and Adams4. These methods are also examined in [24], where the stiffly stable schemes are the BDF-schemes here.

For the Adams2 method, it follows from Table 2 that the solution $\hat{u}^n$ of order 2 satisfies:

$$(1 + 0.5\vartheta)\hat{u}^{n+1} + (1.5\xi + 0.5\vartheta - 1)\hat{u}^n - 0.5\xi\hat{u}^{n-1} = 0.$$

The characteristic equation for the amplification factor is given by

$$(1 + 0.5\vartheta)z^2 + (1.5\xi + 0.5\vartheta - 1)z - 0.5\xi = 0.$$

The same arguments as for the BDF2 method in Proposition 1 lead to the following equation for ξ_*:

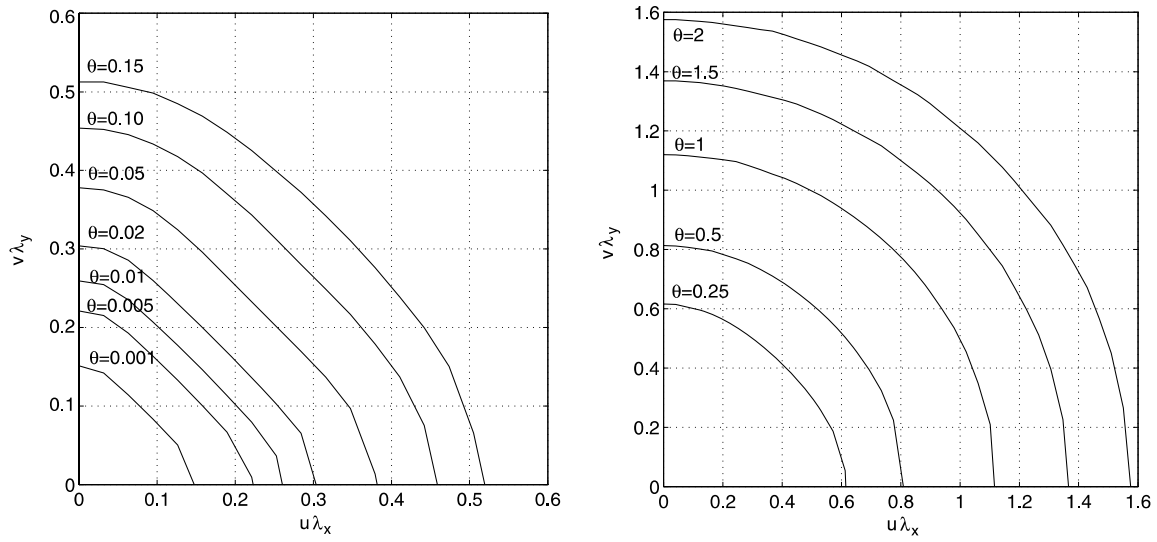

Fig. 2. Stability domain for BDF2 and different θ. Close-up view for small θ (left) and for larger θ (right).

$$\xi_* = -\mathrm{i}\frac{-6\vartheta + 2\sqrt{\vartheta(16+9\vartheta)} - 3\vartheta^2 + \vartheta\sqrt{\vartheta(16+9\vartheta)}}{\sqrt{8\sqrt{\vartheta(16+9\vartheta)} - 6\vartheta^2 + 2\vartheta\sqrt{\vartheta(16+9\vartheta)} - 8\vartheta}}. \tag{24}$$

In Fig. 3(a) and (b), the boundary of the stability domain has been calculated for the same values of θ as in the semi-explicit BDF2 scheme. Similar calculations lead to stability domains for the other schemes. The BDF1 method is considered in Fig. 3(c) and (d). Higher order BDF and Adams methods are considered in Figs. 4 and 5. The methods are stable for points $(\bar{u}\lambda_x, \bar{v}\lambda_y)$ inside the contours. Closed expressions such as in (23) and (24) are not available for the third and fourth order methods. The roots of the characteristic equations are computed numerically.

For the higher order BDF schemes, as θ decreases the stability domain approaches the triangles $(\bar{u}\lambda_x + \bar{v}\lambda_y) \leqslant 0.367$ for BDF3 and $(\bar{u}\lambda_x + \bar{v}\lambda_y) \leqslant 0.313$ for BDF4. For the Adams methods, the stability domain grows for decreasing θ. Adams3 and Adams4 become unstable for $\theta > \frac{1}{2}$ and $\theta > \frac{1}{4}$, respectively. This is due to the fact that the stability domain of the higher order implicit Adams methods does not include the entire negative real axis [22]. The stability domains are limited from above by $(\bar{u}\lambda_x + \bar{v}\lambda_y) \leqslant 0.416$ for Adams3 and $(\bar{u}\lambda_x + \bar{v}\lambda_y) \leqslant 0.243$ for Adams4. The Adams3 scheme was deemed "inappropriate for all practical reasons" in [24].

For fully explicit methods, the stability analysis can be simplified and a standard scalar stability analysis as in [22] can be applied.

3.3. Projection methods

In the previous subsection, we have assumed that the equations for u^{n+1}, v^{n+1} and p^{n+1} are solved simultaneously. Another way of solving the Navier–Stokes equations is to decouple the equations for the velocity and the pressure by using projection methods. The classical projection method [13,41] is

$$\frac{\mathbf{w}^* - \mathbf{w}^n}{\Delta t} = Re^{-1}\Delta_h \mathbf{w}^* - \mathcal{N}_h(\mathbf{w}^n), \tag{25}$$

$$\frac{\mathbf{w}^{n+1} - \mathbf{w}^*}{\Delta t} = -\nabla_h p^{n+1}, \tag{26}$$

$$\nabla_h \cdot \mathbf{w}^{n+1} = 0. \tag{27}$$

The subscript h denotes the discretized spatial operators introduced in Section 2. In practice the equations are solved by taking the discrete divergence of (26) which results in a Poisson equation for the pressure. The scheme is first order accurate and can be written as

$$\frac{\mathbf{w}^{n+1} - \mathbf{w}^n}{\Delta t} = -\nabla_h p^{n+1} + Re^{-1}\Delta_h(\mathbf{w}^{n+1} + \Delta t\nabla_h p^{n+1}) - \mathcal{N}_h(\mathbf{w}^n), \tag{28}$$

$$\nabla_h \cdot \mathbf{w}^{n+1} = 0. \tag{29}$$

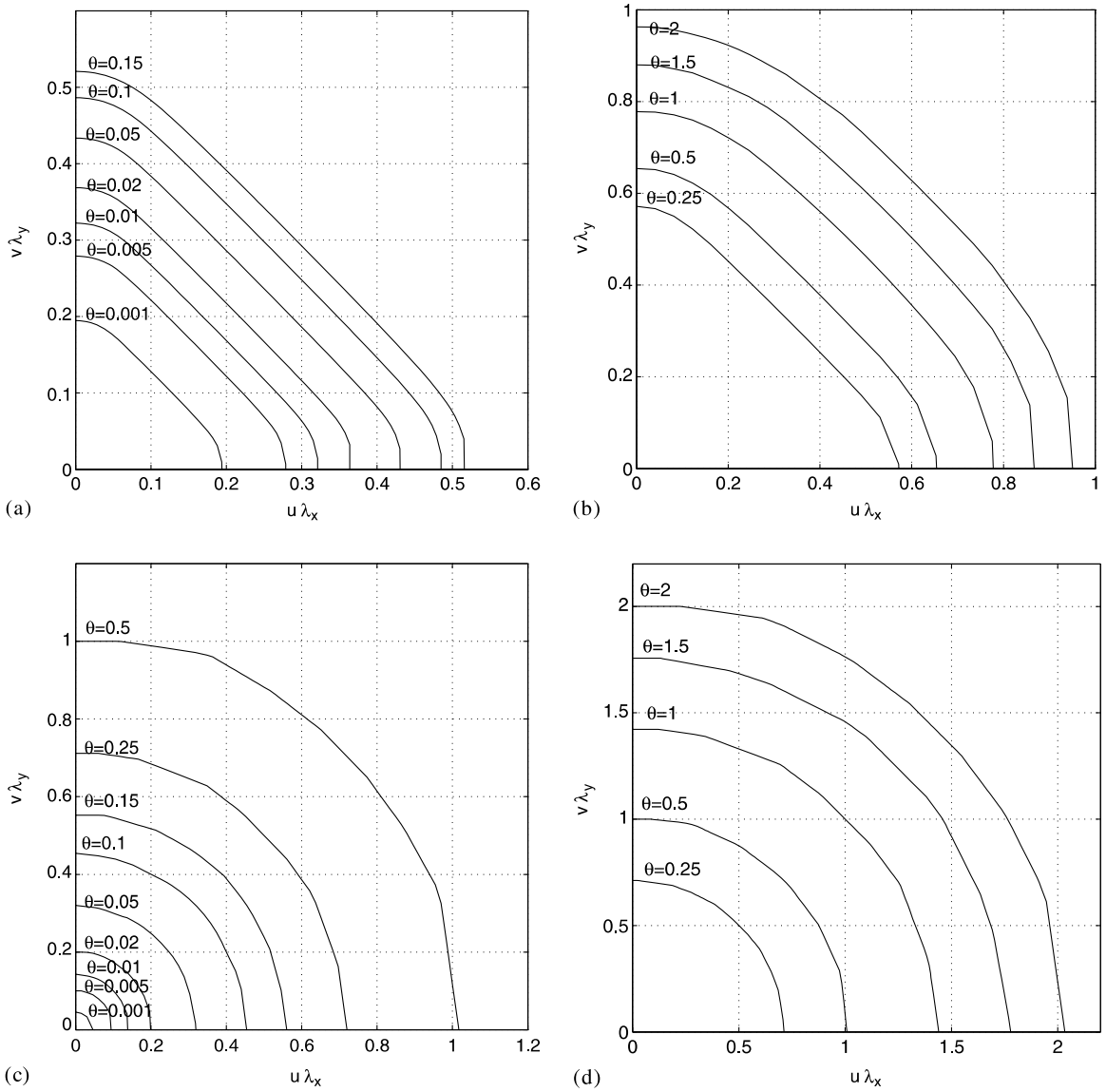

Fig. 3. Stability domain for Adams2 and BDF1 and different θ. Close-up view for small θ (left) and for larger θ (right). (a,b) Adams2 and (c,d) BDF1.

We can now perform a similar analysis as in the beginning of Section 3. Fourier transformation in space yields the following transformed equation for $\hat{u}$ and the same equation for $\hat{v}$:

$$\hat{u}^{n+1} - \hat{u}^n + (\bar{u}\lambda_x a_1 + \bar{v}\lambda_y a_2)\hat{u}^n + \lambda_x b_1(1 + \theta c_0 \Delta t)\hat{p}^{n+1} = -\theta c_0 \hat{u}^{n+1}.$$

This is the same equation as (17a) for the BDF1 scheme with $\lambda_x b_1 \hat{p}^{n+1}$ replaced by $\lambda_x b_1(1 + \theta c_0 \Delta t)\hat{p}^{n+1}$. It follows that the stability domain is the same as for the original BDF1 scheme in Fig. 3(c) and (d).

A way to achieve a second order accurate projection method is to use the pressure increment scheme [4,26,23]

$$\frac{\mathbf{w}^* - \mathbf{w}^n}{\Delta t} = -\nabla_h p^{n-1/2} + \frac{1}{2} Re^{-1} \Delta_h (\mathbf{w}^* + \mathbf{w}^n) - \mathcal{N}_h(\mathbf{w}^{n+1/2}), \tag{30}$$

$$\frac{\mathbf{w}^{n+1} - \mathbf{w}^*}{\Delta t} = -\nabla_h \phi^{n+1}, \tag{31}$$

$$\nabla_h \cdot \mathbf{w}^{n+1} = 0, \tag{32}$$

$$p^{n+1/2} = p^{n-1/2} + \phi^{n+1} - Re^{-1} \frac{\Delta t}{2} \Delta_h \phi^{n+1}. \tag{33}$$

The nonlinear term in (30) is an approximation at time level $t^{n+1/2}$, which is calculated explicity. The stability of the pressure correction scheme depends highly on the method used to compute $\mathbf{w}^{n+1/2}$, see [31].

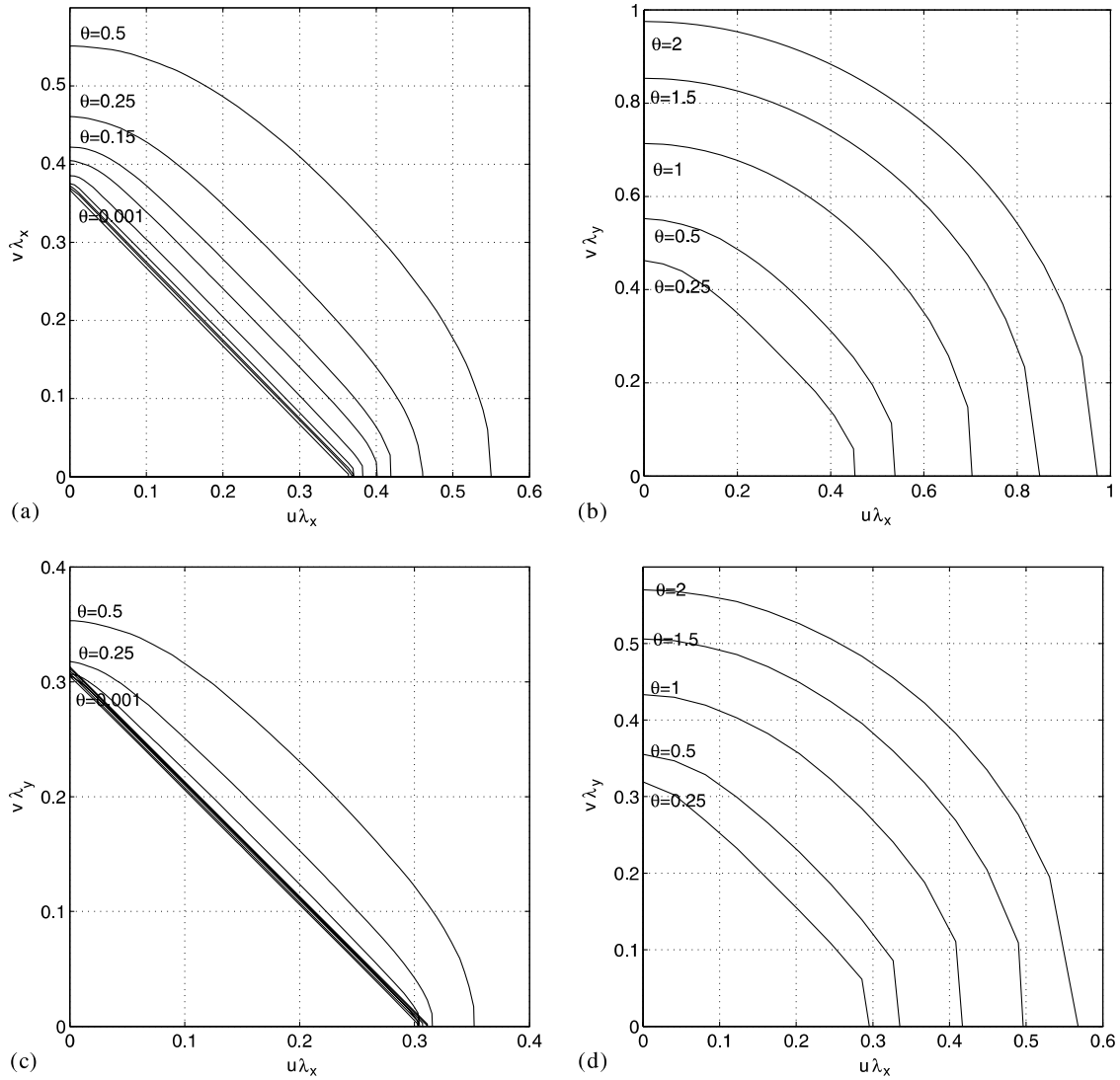

Fig. 4. Stability domain for higher order BDF schemes and different θ. Close-up view for small θ (left) and for larger θ (right). (a,b) BDF3 and (c,d) BDF4.

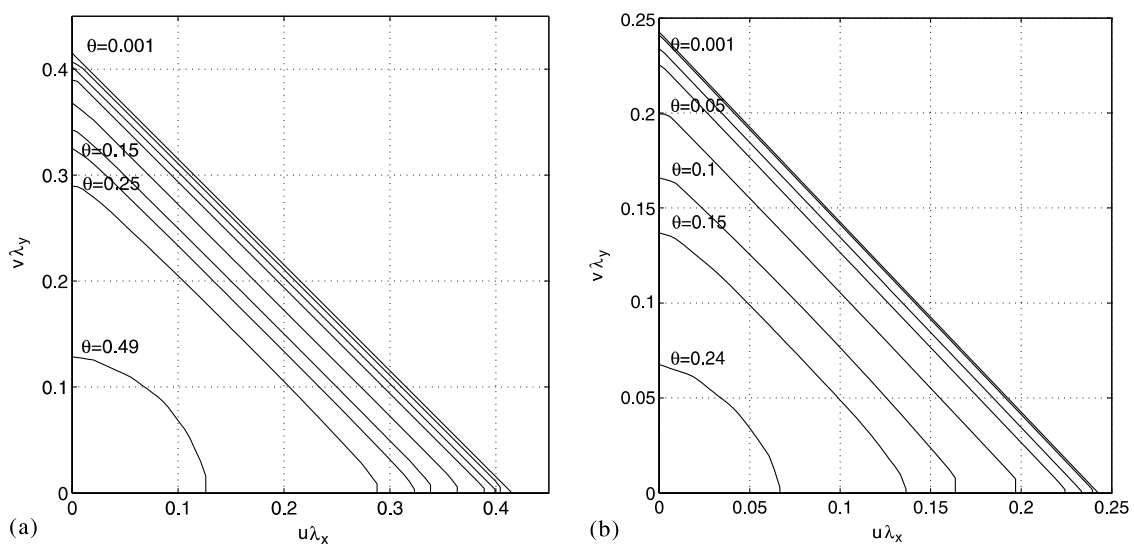

Fig. 5. Stability domain for higher order Adams methods and different θ. (a) Adams3 and (b) Adams4.

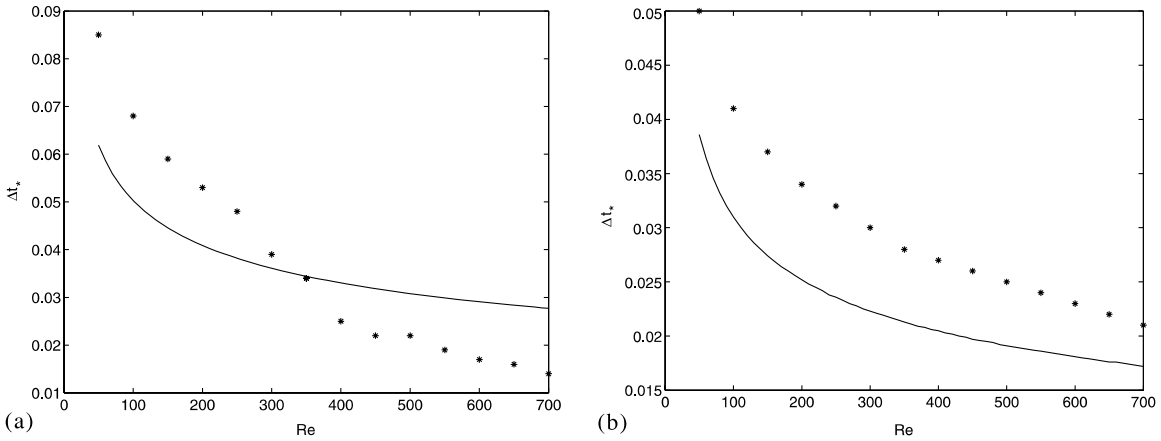

Fig. 6. Theoretically (solid) and experimentally (∗) obtained maximal time steps for stability in a straight channel. (a) $N_x = 24$ and (b) $N_x = 48$.

3.4. Stability for the nonlinear Navier–Stokes equations

The stability analysis above has been obtained for the linearized Navier–Stokes equations with periodic boundary conditions using Fourier representation. We now compare the results obtained by the linear stability analysis to numerical experiments using the Navier–Stokes solver in [7] in a straight channel geometry with $(x, y) \in [-\pi, \pi] \times [-\pi, \pi]$. We impose boundary conditions and initial conditions in form of a Poiseuille profile with a small oscillatory perturbation in the y-direction with the frequency ω_y

$$
\begin{aligned}
&u(x, y, 0) = (1 - y^2/\pi^2) + 0.2\sin(\omega_y y),\\
&v(x, y, 0) = 0.2\sin(\omega_y y),\\
&u(-\pi, y, t) = u(\pi, y, t) = (1 - y^2/\pi^2) - 0.2\sin(\omega_y y),\\
&v(-\pi, y, t) = v(\pi, y, t) = -0.2\sin(\omega_y y),\\
&u(x, -\pi, t) = u(x, \pi, t) = 0,\\
&v(x, -\pi, t) = v(x, \pi, t) = 0.
\end{aligned}
$$

From the linear stability analysis we can calculate the least stable modes. For most values of θ, taking $\omega_y \approx N_y/4$, where N_y is the number of grid points in the y-direction, results the least stable modes.

For $\omega_y = N_y/4$ and for fixed Δx and $\Delta x = \Delta y$, we have determined the maximal time step Δt_* for which the solution is stable during a time interval of about 1500 time steps. The experimental results are compared to the results obtained from the linear stability analysis. The results are shown in Fig. 6, where the experimental results are marked by ∗ and the results from the linear stability analysis using $\bar{u} = 1.2$ and $\bar{v} = 0.2$ are given by the solid line. The first observation is that for large spatial step sizes and large Re, the linear stability analysis does not predict the stability of the fully nonlinear Navier–Stokes equations very well in Fig. 6(a). This is probably caused by the poor resolution in the boundary layer and nonlinear effects. Otherwise, the maximal time steps for the test example lie 20–30% below the predicted time steps. The rate of change of the maximal Δt depending on Re is well predicted by the linear stability analysis. The predictions of the Fourier analysis is also in good agreement with numerical experiments in more complicated geometries in [40].

4. Accuracy

In this section the length and time scales for turbulent flow in a boundary layer are investigated to estimate the spatial step Δx and the time step Δt required for a sufficient accuracy in the discretization. The geometry is typically a straight channel. The assumption is that certain numbers of grid points, n_l and n_t, are needed to resolve the length scale and the time scale, respectively. The numbers n_l and n_t depend on the order of accuracy of the discretization. Then the CFL-number $u\lambda_x$ and θ can be estimated.

Let u_τ be the friction velocity defined by $\sqrt{\nu \partial u/\partial y}$ at a wall with y increasing in the normal direction. In near-wall turbulence the length scale ℓ_w is $y^+ = u_\tau \ell_w/\nu = 1$, [19,44], i.e., $\ell_w = \nu/u_\tau$, and the time scale is $t_w = \ell_w/u_\tau = \nu/u_\tau^2$. Introduce the quotient $\chi = u_b/u_\tau$ between the base flow velocity and the friction velocity. In dimensionless quantities the scales L_w and T_w at the solid wall are now

$$
L_w = \frac{\ell_w}{\ell} = \frac{\nu}{u_\tau \ell} = \frac{\chi}{Re}, \quad T_w = \frac{t_w u_b}{\ell} = \frac{\nu u_b}{u_\tau^2 \ell} = \frac{\chi^2}{Re}. \tag{34}
$$

Assume that we need n_t time steps Δt to resolve the time scale and n_l space steps Δx to resolve the length scale. Then at the wall

$$\Delta x_{\mathrm{w}} = \frac{L_{\mathrm{w}}}{n_l} = \frac{\chi}{n_l Re}, \quad \Delta t_{\mathrm{w}} = \frac{T_{\mathrm{w}}}{n_t} = \frac{\chi^2}{n_t Re} = \chi \frac{n_l}{n_t} \Delta x_{\mathrm{w}}. \tag{35}$$

The quotient χ varies slowly with Re. In DNS experiments in a channel in [1] χ is about 15 in a case with $Re = 1955$ and increases to 17 when $Re = 6210$. The measured data in a channel in [35] show a growth in χ from 25 to 31 when Re increases from 5000 to 30,000. In turbulent pipe flow at $Re = 5317$ in [19] $\chi = 15$. The friction coefficient c_{f} is defined by

$$c_{\mathrm{f}} = u_\tau^2/(0.5u_b^2) = 2\chi^{-2}$$

for turbulent flow over a flat plate with $Re > 10^5$. It satisfies the empirical relation

$$c_{\mathrm{f}} = 0.0576 u_b \nu^{-1} x^{-1/5},$$

where x is the position in the downstream direction on the plate [39]. Combining the two expressions for c_{f} the result for χ is

$$\chi = 5.9 Re^{0.1} (x/\ell)^{0.1},$$

which is about 19 for $Re = 10^5$ and $x = \ell$. Hence, by (35) usually $\Delta t_{\mathrm{w}} > \Delta x_{\mathrm{w}}$.

It follows that at the wall

$$\begin{aligned} u\lambda_{\mathrm{w}} &= \frac{u_\tau}{u_b}\lambda_{\mathrm{w}} = \chi^{-1}\frac{\Delta t_{\mathrm{w}}}{\Delta x_{\mathrm{w}}} = \chi^{-1}\frac{T_{\mathrm{w}} n_l}{L_{\mathrm{w}} n_t} = \frac{n_l}{n_t}, \\ \theta_{\mathrm{w}} &= \frac{\Delta t_{\mathrm{w}}}{Re \Delta x_{\mathrm{w}}^2} = \frac{n_l^2}{n_t}. \end{aligned} \tag{36}$$

For good accuracy in time and space with a second order method in time and a fourth order method in space we need, say, $n_t = 10$ and $n_l = 4$, see [28]. Hence, $u\Delta t_{\mathrm{w}}/\Delta x_w = 0.4$. In [12], the time steps are found in numerical experiments in a plane channel to be such that $n_t \approx 5$ in a second order method similar to the Crank–Nicolson method. The CFL-number for good accuracy is there rather low, 0.5–1.

A much smaller time step is necessary for high accuracy in other flow regimes, such as transitional flow [19].

5. Iterative method

In every time step with a semi-explicit method, a system of linear equations has to be solved for $(\mathbf{w}^{n+1}, p^{n+1})$ at the N grid points. Let $\tilde{\mathbf{w}}^{n+1} \in \mathbb{R}^{2N}$ and $\tilde{p}^{n+1} \in \mathbb{R}^N$ be the solution vectors. Then let $D\tilde{\mathbf{w}}^{n+1}$ approximate the divergence of the velocity, $G\tilde{p}^{n+1}$ the gradient of the pressure, and $L\tilde{\mathbf{w}}^{n+1}$ the Laplacian applied to the velocity components. Here

$$D \in \mathbb{R}^{N\times 2N}, G \in \mathbb{R}^{2N\times N}, L \in \mathbb{R}^{2N\times 2N},$$

and A is defined by

$$A = \alpha_0 I - Re^{-1}\Delta t \beta_0^i L. \tag{37}$$

The new solution at t^{n+1} satisfies

$$\begin{pmatrix} A & \Delta t\beta_0^i G \\ D & 0 \end{pmatrix} \begin{pmatrix} \tilde{\mathbf{w}}^{n+1} \\ \tilde{p}^{n+1} \end{pmatrix} = \begin{pmatrix} \mathbf{b}_1 \\ b_2 \end{pmatrix}, \tag{38}$$

where $\mathbf{b}_1$ and b_2 depend on previous solutions $\tilde{\mathbf{w}}^{n-i}$, $\tilde{p}^{n-i}$, $i = 0, 1, 2\ldots$, and the boundary conditions. The structure of (38) is the same, independent of the time stepping method in Section 3.

Two different approaches to solution of (38) are investigated here:

1. An approximate factorization of the system matrix is introduced as in [7,11,14,36].
2. An exact factorization of the matrix defines a Schur complement system of linear equations for the pressure as in [10,17,43].

An overview and a discussion of different factorizations of the matrix in (38) in the same spirit as below is found in [37].

In the first case an LU-factorization of a nearby matrix is computed

$$\begin{pmatrix} A & \Delta t\beta_0^i G \\ D & 0 \end{pmatrix} \approx \begin{pmatrix} A & 0 \\ D & -\alpha_0^{-1}\Delta t\beta_0^i DG \end{pmatrix} \begin{pmatrix} I & \alpha_0^{-1}\Delta t\beta_0^i G \\ 0 & I \end{pmatrix} = \begin{pmatrix} A & \alpha_0^{-1}\Delta t\beta_0^i AG \\ D & 0 \end{pmatrix}. \tag{39}$$

To compute $\tilde{\mathbf{w}}^{n+1}$ and $\tilde{p}^{n+1}$ with the approximate factorization, two systems of linear equations have to be solved in a forward and a backward substitution sweep

$$\begin{aligned}&1.\quad A\mathbf{w}^* = \mathbf{b}_1,\\ &2.\quad DG\tilde{p}^{n+1} = \alpha_0(\Delta t\beta_0^i)^{-1}(D\mathbf{w}^* - b_2),\\ &3.\quad \tilde{\mathbf{w}}^{n+1} = \mathbf{w}^* - \alpha_0^{-1}\beta_0^i\Delta tG\tilde{p}^{n+1}.\end{aligned} \tag{40}$$

In [11,14,36] these values of $\tilde{\mathbf{w}}^{n+1}$ and $\tilde{p}^{n+1}$ are accepted but in [7] an outer iteration ensures that (38) is solved with sufficient accuracy.

A pressure correction method and the projection method (26) generate the same systems of equations to solve as in (40), see Section 3.3 and [2,4,6,15,41,23].

An exact factorization of the matrix in (38) is

$$\begin{pmatrix} A & \Delta t\beta_0^i G\\ D & 0\end{pmatrix} = \begin{pmatrix} A & 0\\ D & -\Delta t\beta_0^i DA^{-1}G\end{pmatrix}\begin{pmatrix} I & \Delta t\beta_0^i A^{-1}G\\ 0 & I\end{pmatrix}. \tag{41}$$

In the second alternative, the steps to solve (38) for the velocity and the pressure are

$$\begin{aligned}&1.\quad A\mathbf{w}^* = \mathbf{b}_1,\\ &2.\quad DA^{-1}G\tilde{p}^{n+1} = (\Delta t\beta_0^i)^{-1}(D\mathbf{w}^* - b_2),\\ &3.\quad \tilde{\mathbf{w}}^{n+1} = \mathbf{w}^* - \beta_0^i\Delta tA^{-1}G\tilde{p}^{n+1}.\end{aligned} \tag{42}$$

The inverse of A is dense and is not computed and stored. In an iterative solution of step 2 in (42) with a Krylov method where the multiplication of an arbitrary vector f with $DA^{-1}G$ is needed, either A^{-1} is approximated [17,43] or a system of equations is solved

$$Ag = Gf$$

to compute $DA^{-1}Gf = Dg$. In step 1, the system is solved by an iterative method. The system in step 3 is solved either with an approximation of A^{-1} or by an iterative method after multiplying the left and right hand sides with A. The approximation of A^{-1} in step 2 may be different from the one in step 3. With $A^{-1} = \alpha_0^{-1}I$ in (42) the methods in (40) and (42) coincide.

Sufficient accuracy in the solution of (38) is obtained by solving it iteratively using the approximate factorization (39) [7] or the exact factorization (41) with an approximation of A^{-1} [43]. Let the original system (38) be

$$Mx = b, \tag{43}$$

where $x = (\tilde{\mathbf{w}}^{n+1}, \tilde{p}^{n+1})^{\mathrm{T}}$ and $b = (\mathbf{b}_1^{\mathrm{T}}, b_2^{\mathrm{T}})^{\mathrm{T}}$, and denote the approximate factorization matrix (39) or an approximation of the factorization (41) by $\widetilde{M}$. Then

$$\widetilde{M} = \begin{pmatrix} A & 0\\ D & -\Delta t\beta_0^i DBG\end{pmatrix}\begin{pmatrix} I & \Delta t\beta_0^i BG\\ 0 & I\end{pmatrix}, \tag{44}$$

where $B = \alpha_0^{-1}I$ in (39) and $B = A^{-1}$ or B approximates A^{-1} in (41).

To solve (43), we use a fixed point iteration with $\widetilde{M}$ as a preconditioner in an outer iteration, i.e.,

$$x^{(k+1)} = x^{(k)} + \delta x^{(k)} = x^{(k)} + \widetilde{M}^{-1}(b - Mx^{(k)}) = x^{(k)} + \widetilde{M}^{-1}r^{(k)}, \tag{45}$$

or

$$r^{(k+1)} = b - Mx^{(k+1)} = (I - M\widetilde{M}^{-1})r^{(k)}.$$

The analysis of the spectral radius of $I - M\widetilde{M}^{-1}$ in [43] reveals that it is less than 1 for all Δt but that it approaches 1 when Δt increases. There is no time step restriction imposed by the outer iteration (45) for convergence but the efficiency is hampered by too large a Δt.

Other approximations of the Schur complement $DA^{-1}G$ in the preconditioner in (44) are examined for the steady state problem in [18,25]. The system of linear Eq. (43) is solved by preconditioned GMRES [38] and the number of iterations are almost independent of the grid size Δx and increase slowly with increasing Re. The convergence with a multigrid algorithm is proved to be independent of Δx and Re for a convection–diffusion equation in [34]. However, the convergence properties of iterative methods for the steady state solution and the time-dependent solution are often different. The spectral radius of $DA^{-1}G$ with $A \sim L$ is of $\mathcal{O}(1)$ for the steady state problem but this is not the case when A is as in (37). The different behavior of the preconditioner in [25] applied to a steady state problem and an unsteady problem is observed in [16].

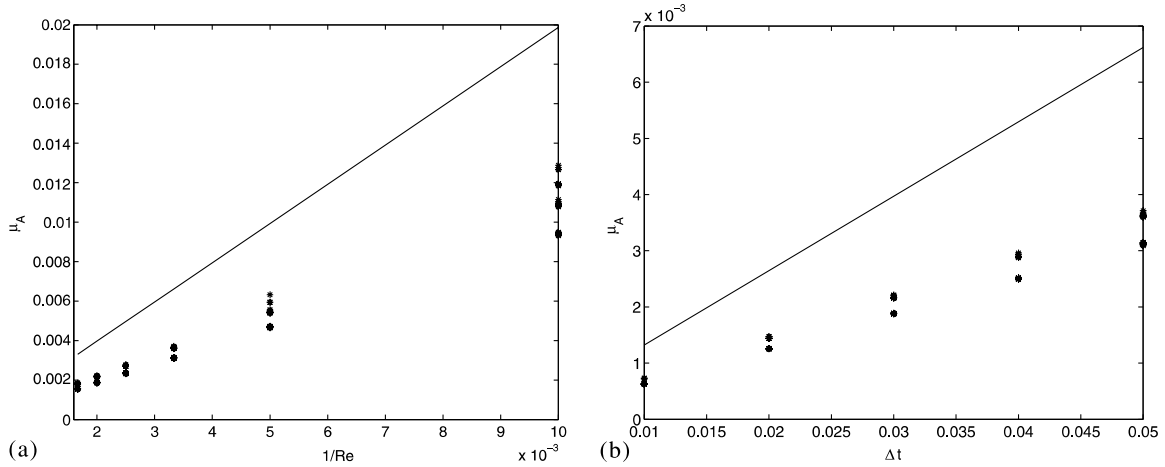

Fig. 7. Amplification factor μ_A in (46). The theoretical estimate of μ_A (solid line) is compared to experimental values (∗). (a) $\Delta t = 0.05$ and (b) $Re = 300$.

Fixed point iteration is an option to solve the momentum Eq. (40) in [7]. For the residual ρ we have

$$\rho^{(l+1)} = \mathbf{b}_1 - A\mathbf{w}^{(l+1)} = \mathbf{b}_1 - A(\mathbf{w}^{(l)} + \widetilde{A}^{-1}(\mathbf{b}_1 - A\mathbf{w}^{(l)})) = (I - A\widetilde{A}^{-1})\rho^{(l)}$$

with the preconditioner $\widetilde{A}^{-1}$. The iteration for the first inner system with $\widetilde{A}^{-1} = \alpha_0^{-1} I$ converges if

$$\mu_A = \|I - A\widetilde{A}^{-1}\| = \alpha_0^{-1}\Delta t \beta_0^i Re^{-1}\|L\| < 1. \tag{46}$$

If L is symmetric, then Δt must satisfy $\Delta t < \alpha_0 Re/(\beta_0^i \max_i|\lambda_i(L)|)$, where λ_i is an eigenvalue of L. With periodic solutions, Fourier analysis yields $\|L\| \leqslant 12/\Delta x^2$, and the iterations converge if

$$\theta = \Delta t/(Re\Delta x^2) < \alpha_0(\beta_0^i)^{-1}/12. \tag{47}$$

For given Δx and Re, this introduces a strict limit on the admissible time step. The theoretical results for the amplification factor μ_A in (46) are compared to numerical tests using the Navier–Stokes solver in [7]. In Fig. 7(a) and (b), we have plotted μ_A as a function of Re^{-1} and Δt, respectively. The solid curve represents the maximum eigenvalue obtained by Fourier analysis. The values of $\|\rho_1^{(l)}\|/\|\rho_1^{(l-1)}\|$ obtained from numerical experiments in a straight channel are marked by ∗. The boundary and initial data are the eigenfunctions which correspond to the largest eigenvalues in the Fourier analysis. The theoretically determined μ_A based on periodic boundary conditions always overestimates the actual amplification factor in the experiments. The linear dependence on Δt and $1/Re$ is clearly visible in the experimental data.

The number of iterations to reach convergence grows slowly with increasing Δt in [16] for the time-dependent driven cavity problem. When Δt is 16 times as large, the number of iterations in every time step is about twice as large. By using BiCGSTAB [44] for both the momentum and the pressure equations, the time step is restricted by the stability and the accuracy in experiments in [40]. The unsteady three-dimensional Navier–Stokes equations are solved in [17] with encouraging results. Both the momentum equation and the pressure equation in (42) are solved by multigrid iteration and the preconditioner in [25]. The number of iterations is insensitive to the time step when time accurate solutions are computed and it is independent of Re. With such a solver in each time step, only accuracy and stability restricts the length of Δt.

6. Conclusions

The stability of different semi-explicit time discretizations of the incompressible Navier–Stokes equations has been investigated with a model system of equations in Fourier space. The size of the stability domain for the CFL-numbers $u\lambda_x$ and $v\lambda_y$ depends on the parameter $\theta = \Delta t/(Re\Delta x^2)$. The time step limits with the linear theory overestimate the limits obtained experimentally with a solver of the Navier–Stokes equations, but the trend is correctly predicted.

The time and length scales for wall bounded turbulent flow are derived. The number of points per unit length is chosen depending on the order of the method yielding Δt and Δx. The requirements on $u\lambda_x$ and θ for sufficient accuracy in the boundary layer depend only on the number of points needed to resolve the scales in time and space. This number depends on the accuracy of the discretization.

One system of linear equations is solved iteratively in each time step for the velocity and the pressure in an outer iteration and two or three inner iterations. The equations to be solved in every outer iterative step are similar for most strategies to solve the Navier–Stokes equations. Depending on the choice of iterative method, there may be a bound on the time step for convergence, the convergence rate may be slower for larger Δt or it may be independent Δt as demonstrated by a multigrid solver in [17].

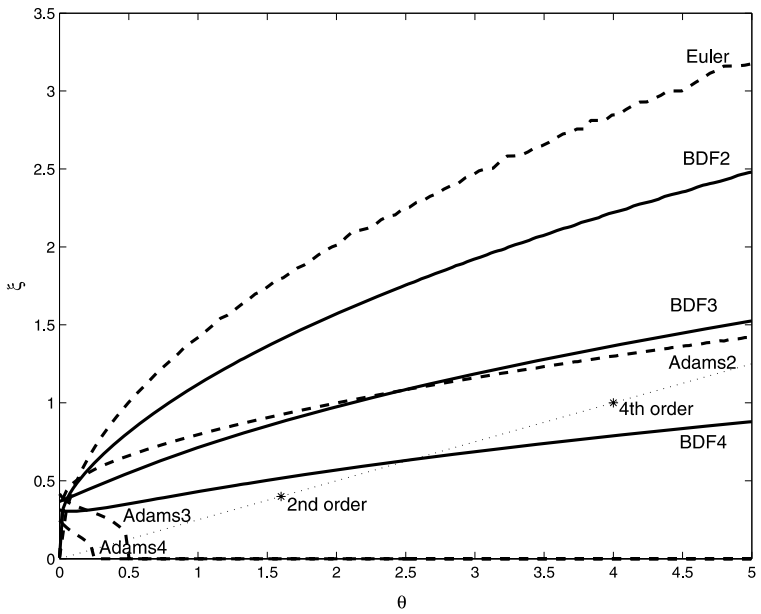

Fig. 8. The stability bounds for different time discretizations.

The stability domains for the semi-implicit methods of the BDF and Adams families up to fourth order are displayed in Fig. 8. The bound on the CFL-number $\xi = u\lambda_x$ with $v = 0$ is plotted as a function of θ. The BDF methods have better stability properties than their Adams counterpart of the same order. The stability domains in Fig. 8 for BDF2, BDF3, and Adams2 agree well with the domains in [3] for a simpler model problem. The requirements for sufficient accuracy on ξ and θ in a turbulent boundary layer are marked by $*$ for the discretizations of fourth order in space ($n_l = 4$ in (36)) and second ($n_t = 10$) and fourth ($n_t = 4$) order in time. The second order mark is well within the stability domain for BDF2. Accuracy decides which ξ and θ to choose and Δt is given by ξ, θ, and (36). The ξ and θ for sufficient accuracy in the fourth order case are not stable with BDF4. By decreasing Δt so that ξ and θ move along the dotted line, they are inside the stability domain at about $\theta = 2.5$ and the scheme is then both accurate and stable. Stability determines the largest possible time step in this case. Note that it is possible to decrease Δt in this way and obtain stability for all the methods in the figure, no matter what the accuracy requirements are on ξ and θ.

With an iteration that converges independently of the time step we can expect: the total work decreases with longer time steps. Then the bound on Δt is imposed by accuracy or stability. From Fig. 8 we conclude that BDF4 allows larger θ (and Δt) than BDF2 and therefore appears to be the most efficient alternative for wall bounded turbulent flow. The only disadvantage with BDF4 is that two more solution vectors must be stored.

Acknowledgement

Valuable input to the discussion in Section 4 was provided by Arne Johansson and Arnim Brüger pointed out Refs. [1,35] to us. This work was supported by the Swedish Foundation for Strategic Research.

References

[1] K. Alvelius, Studies of turbulence and its modelling through large Eddy- and direct numerical simulation, Ph.D. thesis, Dept. of Mechanics, Royal Institute of Technology, Stockholm, Sweden, 1999.
[2] S. Armfield, R. Street, The fractional-step method for the Navier–Stokes equations on staggered grids: The accuracy of three variations, J. Comput. Phys. 153 (1999) 660–665.
[3] U.M. Ascher, S.J. Ruuth, B.T.R. Wetton, Implicit–explicit methods for time-dependent partial differential equations, SIAM J. Numer. Anal. 32 (1995) 797–823.
[4] J.B. Bell, P. Colella, H.M. Glaz, A second-order projection method for the incompressible Navier–Stokes eqautions, J. Comput. Phys. 85 (1989) 257–283.
[5] K. Bhaganagar, D. Rempfer, J. Lumley, Direct numerical simulation of spatial transition to turbulence using fourth-order vertical velocity second-order vertical vorticity formulation, J. Comput. Phys. 180 (2002) 200–228.
[6] D.L. Brown, R. Cortez, M.L. Minion, Accurate projection methods for the incompressible Navier–Stokes equations, J. Comput. Phys. 168 (2001) 464–499.
[7] A. Brüger, B. Gustafsson, P. Lötstedt, J. Nilsson, High order accurate solution of the incompressible Navier–Stokes equations, J. Comput. Phys. 203 (2005) 49–71.

[8] A. Brüger, B. Gustafsson, P. Lötstedt, J. Nilsson, Splitting methods for high order solution of the incompressible Navier–Stokes equations in 3D, Int. J. Numer. Meth. Fluids 47 (2005) 1157–1163.
[9] A. Brüger, J. Nilsson, W. Kress, A compact higher order finite difference method for the incompressible Navier–Stokes equations, J. Sci. Comput. 17 (2002) 551–560.
[10] J. Cahouet, J.-P. Chabard, Some fast 3D finite element solvers for the generalized Stokes problem, Int. J. Numer. Meth. Fluids 8 (1988) 869–895.
[11] W. Chang, F. Giraldo, B. Perot, Analysis of an exact fractional step method, J. Comput. Phys. 180 (2002) 183–199.
[12] H. Choi, P. Moin, Effects of the computational time step on numerical solutions of turbulent flow, J. Comput. Phys. 113 (1994) 1–4.
[13] A.J. Chorin, Numerical solution of the Navier–Stokes equations, Math. Comput. 22 (1968) 745–762.
[14] J.K. Dukowicz, A.S. Dvinsky, Approximate factorization as a high order splitting for the implicit incompressible flow equations, J. Comput. Phys. 102 (1992) 336–347.
[15] W. E, J.-G. Liu, Projection method I: Convergence and numerical boundary layers, SIAM J. Numer. Anal. 32 (1995) 1017–1057.
[16] H.C. Elman, Preconditioners for saddle point problems arising in computational fluid dynamics, Appl. Numer. Math. 43 (2002) 75–89.
[17] H.C. Elman, V.E. Howle, J.N. Shadid, R.S. Tuminaro, A parallel block multi-level preconditioner for the 3D incompressible Navier–Stokes equations, J. Comput. Phys. 187 (2003) 504–523.
[18] H.C. Elman, D.J. Silvester, A.J. Wathen, Performance and analysis of saddle point preconditioners for the discrete steady-state Navier–Stokes equations, Numer. Math. 90 (2002) 665–688.
[19] R. Friedrich, T.J. Hüttl, M. Manhart, C. Wagner, Direct numerical simulation of incompressible turbulent flows, Comput. Fluids 30 (2001) 555–579.
[20] B. Gustafsson, P. Lötstedt, A. Göran, A fourth order difference method for the incompressible Navier–Stokes equations, in: M.M. Hafez (Ed.), Numerical Simulations of Incompressible Flows, World Scientific Publishing, Singapore, 2003, pp. 263–276.
[21] E. Hairer, S.P. Nørsett, G. Wanner, Solving Ordinary Differential Equations I, Nonstiff Problems, second ed., Springer-Verlag, Berlin, 1993.
[22] E. Hairer, G. Wanner, Solving Ordinary Differential Equations II, Stiff and Differential-Algebraic Problems, second ed., Springer-Verlag, Berlin, 1996.
[23] J. van Kan, A second-order accurate pressure correction scheme for viscous incompressible flow, SIAM J. Sci. Stat. Comput. 7 (1986) 870–891.
[24] G.E. Karniadakis, M. Israeli, S.A. Orszag, High-order splitting methods for incompressible Navier–Stokes equations, J. Comput. Phys. 97 (1991) 414–443.
[25] D. Kay, D. Loghin, A. Wathen, A preconditioner for the steady-state Navier–Stokes equations, SIAM J. Sci. Comput. 24 (2002) 237–256.
[26] J. Kim, P. Moin, Application of a fractional-step method to incompressible Navier–Stokes equations, J. Comput. Phys. 59 (1985) 308–323.
[27] W. Kress, J. Nilsson, Boundary conditions and estimates for the linearized Navier–Stokes equations on a staggered grid, Comput. Fluids 32 (2003) 1093–1112.
[28] S.K. Lele, Compact finite difference schemes with spectral-like resolution, J. Comput. Phys. 103 (1992) 16–42.
[29] R. Löhner, Multistage explicit advective prediction for projection-type incompressible flow solvers, J. Comput. Phys. 195 (2004) 143–152.
[30] A. Lundbladh, D.S. Henningson, A.V. Johansson, An efficient spectral integration method for the solution of the time-dependent Navier–Stokes equations, Report FFA-TN 1992-28, Aeronautical Research Institute of Sweden, Bromma, Sweden, 1992.
[31] M.L. Minion, On the stability of Godunov-projection methods for incompressible flow, J. Comput. Phys. 123 (1996) 435–449.
[32] S. Nagarajan, S.K. Lele, J.H. Ferziger, A robust high-order compact method for large eddy simulation, J. Comput. Phys. 191 (2003) 392–419.
[33] J. Nilsson, B. Gustafsson, P. Lötstedt, A. Brüger, High order difference method on staggered, curvilinear grids for the incompressible Navier–Stokes equations, in: K.J. Bathe (Ed.), Proceedings of Second MIT Conference on Computational Fluid and Solid Mechanics 2003, Elsevier, 2003, pp. 1057–1061.
[34] M.A. Olshanskii, A. Reusken, Convergence analysis of a multigrid method for a convection-dominated model problem, SIAM J. Numer. Anal. 42 (2004) 1261–1291.
[35] J.M. Österlund, Experimental studies of zero pressure-gradient turbulent boundary layer flow, Ph.D. thesis, Dept. of Mechanics, Royal Institute of Technology, Stockholm, Sweden, 1999.
[36] J.B. Perot, An analysis of the fractional step method, J. Comput. Phys. 108 (1993) 51–58.
[37] A. Quarteroni, F. Saleri, A. Veneziani, Factorization methods for the numerical approximation of Navier–Stokes equations, Comput. Methods Appl. Mech. Engrg. 118 (2000) 505–526.
[38] Y. Saad, M.H. Schultz, GMRES: A generalized minimal residual algorithm for solving nonsymmetric linear systems, SIAM J. Sci. Comput. 7 (1986) 856–869.
[39] H. Schlichting, Boundary-Layer Theory, McGraw-Hill, New York, 2001.
[40] E. Stålberg, A high order method for simulation of fluid flow in complex geometries, Licentiate thesis, Dept. of Mechanics, Royal Institute of Technology, Stockholm, Sweden, 2005.
[41] R. Temam, Sur l'approximation de la solution des équations de Navier–Stokes par la méthode des pas fractionnaires, II, Arch. Rational Mech. Anal. 33 (1969) 377–385.
[42] S. Turek, A comparative study of time-stepping techniques for the incompressible Navier–Stokes equations: From fully implicit non-linear schemes to semi-implicit projection methods, Int. J. Numer. Meth. Fluids 37 (1999) 37–47.
[43] A. Veneziani, Block factorized preconditioners for high-order accurate in time approximation of the Navier–Stokes equations, Numer. Meth. Part. Diff. Eq. 19 (2003) 487–510.
[44] H.A. van der Vorst, BiCGSTAB: A fast and smoothly converging variant of Bi-CG for the solution of nonsymmetric linear systems, SIAM J. Sci. Comput. 13 (1992) 631–644.
[44] D.C. Wilcox, Turbulence Modeling for CFD, DCW Industries, La Cañada, CA, 1994.